IOPscience iopscience.iop.org

Home Search Collections Journals About Contact us My IOPscience

Linear and non-linear spectroscopy of Ho^{3+}-doped YVO_4 and $LuVO_4$

This article has been downloaded from IOPscience. Please scroll down to see the full text article.

2005 J. Phys.: Condens. Matter 17 6751

(http://iopscience.iop.org/0953-8984/17/42/013)

View the table of contents for this issue, or go to the journal homepage for more

Download details:
IP Address: 129.252.86.83
The article was downloaded on 28/05/2010 at 06:34

Please note that terms and conditions apply.

INSTITUTE OF PHYSICS PUBLISHING JOURNAL OF PHYSICS: CONDENSED MATTER

J. Phys.: Condens. Matter **17** (2005) 6751–6762 doi:10.1088/0953-8984/17/42/013

Linear and non-linear spectroscopy of Ho^{3+}-doped YVO_4 and $LuVO_4$

R Moncorgé[1], M Velazquez[1], P Goldner[2], O Guillot-Noël[2], H L Xu[3], M Nilsson[3], S Kröll[3], E Cavalli[4] and M Bettinelli[5]

[1] Centre Interdisciplinaire de Recherches sur les Ions et les Lasers (CIRIL), UMR 6637 CEA-CNRS-ENSICAEN, Université de Caen, 6 Boulevard Maréchal Juin, 14050 Caen, France
[2] Laboratoire de Chimie Appliquée de l'Etat Solide, UMR7574 CNRS-ENSCP, 11 rue P. et M. Curie, 75005 Paris, France
[3] Department of Physics, Lund Institute of Technology, PO Box 118, S-22100 Lund, Sweden
[4] Dipartimento di Chimica Generale ed Inorganica, Chimica Analitica e, Chimica Fisica, Università di Parma, Parco Area delle Scienze 17/a, 43100 Parma, Italy
[5] Dipartimento Scientifico e Tecnologico, Università di Verona and INSTM, UdR Verona, Ca'Vignal, Strada Le Grazie 15, 37134 Verona, Italy

E-mail: richard.moncorge@ensicaen.fr

Received 16 June 2005, in final form 13 September 2005
Published 7 October 2005
Online at stacks.iop.org/JPhysCM/17/6751

Abstract

Rare-earth-doped crystals can be attractive materials for quantum information processing, because of the long coherence times that can be expected, in particular, from non-Kramers ions. In this paper, Ho^{3+}-doped yttrium and lutetium vanadate single crystals have been investigated using linear and coherent optical spectroscopy. For Ho^{3+}:YVO_4, the crystal-field levels of the $^5I_8$, $^5F_5$, $^5F_4$ and $^5S_2$ multiplets have been determined and compared with crystal-field level calculations. This allowed us to unambiguously assign most of the observed transitions, although some results suggest that the site symmetry of the Ho^{3+} ion could deviate from D_{2d}. Similar conclusions were reached for Ho^{3+}:$LuVO_4$. Hole burning measurements indicate that the coherence time of the $^5I_8$–$^5F_5$ optical transitions is rather short in both compounds (around 40 ns). Assuming that the coherence is limited by spin interactions, this is accounted for by the high nuclear moment of the nearby vanadium ions, since the large crystal-field level splittings of the $^5I_8$ and $^5F_5$ multiplets do not favour a large enhanced nuclear Zeeman effect.

1. Introduction

Crystalline compounds doped with trivalent rare-earth (RE) ions have great interest mainly thanks to their unique spectroscopic characteristics, including narrow absorption lines, long fluorescence lifetimes and excellent optical coherence properties. These compounds thus have

 © 2005 IOP Publishing Ltd Printed in the UK

large potentials as incoherent as well as coherent light emitters and also for applications in areas such as optical data storage and processing, quantum information and computing and frequency standards. Due to the long metastable lifetime which favours energy storage, crystals doped with trivalent holmium ions such Ho^{3+}:YAG, for example, are used for the production of very efficient and high-energy laser devices operating around 2.1 μm [1]. On the other hand, trivalent holmium is also very attractive because it has only one naturally occurring isotope, ^{165}Ho (nuclear spin 7/2), which makes spectral analysis simpler. The spectroscopic properties of Ho^{3+} have been investigated in the past in several crystalline compounds. There have been, among others, a crystal-field splitting analysis of Ho^{3+} in $YAsO_4$, YVO_4 and $HoPO_4$ [2], a theoretical investigation of hyperfine transition intensities of Ho^{3+} in CaF_2 [3], an experimental observation of hyperfine structure splitting outside the inhomogeneous linewidth in Ho^{3+}:$LaCl_3$ [4] and both an experimental and theoretical study of the energy levels of Ho^{3+} in $CaWO_4$ [5].

However, to the best of our knowledge, only three papers [6–8] have been dedicated to the spectroscopy of Ho^{3+}:YVO_4. For the Ho^{3+}:$LuVO_4$ crystal, no spectral data, not even the position of the energy levels, has been reported so far. Further, the results obtained in the case of Ho^{3+}:YVO_4 were partly contradictory. Therefore, one of the objectives of the present paper was to re-examine the spectroscopy of Ho^{3+}:YVO_4 more carefully, as well as to explore the spectroscopy of Ho^{3+}:$LuVO_4$. For this purpose, the considered energy levels in Ho^{3+}:YVO_4 and Ho^{3+}:$LuVO_4$ were located by recording low-temperature absorption and emission spectra and also by performing a series of crystal-field calculations. The present work was also motivated by the search for good rare-earth candidates as active ions for quantum computing in inorganic crystals [9]. The possibility of scaling the quantum computing scheme used in [9] from a few qubits up to several qubits depends, among other things, on the number of absorbing ions per volume and per frequency channel. This indicates that high concentrations of active ions would be favourable. However, in many cases a high dopant concentration also leads to a corresponding broadening of the inhomogeneous absorption line [10]. Thus, the number of ions per volume and frequency interval will be unchanged. It can be expected that this broadening effect increases with the difference in ionic radius between the dopant ion and the host ion that it substitutes. Therefore it was interesting to investigate compounds where Ho^{3+} substitutes for Y^{3+} and Lu^{3+} as these ions have nearly the same ionic radius (115.5 pm for Ho^{3+}, 115.9 pm for Y^{3+} and 111.7 pm for Lu^{3+} in eight-fold coordination [11]). In such a case, it might be possible to have a 'high' holmium concentration without a corresponding increase of the inhomogeneous line. As ions used as qubits also need to have long coherence times (associated with narrow homogeneous linewidth optical transitions), the prospect of using Ho^{3+} ions as active qubits for quantum computation was further investigated by measuring the homogeneous and inhomogeneous linewidths of the $^5I_8$–$^5F_5$ optical transition by using spectral hole burning techniques.

2. Experiments

The single crystals of Ho^{3+}:YVO_4 and Ho^{3+}:$LuVO_4$ were grown by using the flux method [12]. Their nominal dopant concentrations were 0.5 and 1 at.%. Both crystals have a zircon structure and belong to the tetragonal space group $I4_1/amd$. The Ho^{3+} ions substitute for the Y^{3+} or the Lu^{3+} ions in eight-fold coordination, with the site symmetry $\bar{4}m2$ (D_{2d}), in the crystallographic system abc, or $\bar{4}2m$, in an xyz system rotated by $\pi/2$ around the $c \equiv z$ axis. The samples used in the experiments were about 1 mm thick with two polished faces.

The absorption spectra were measured with the aid of a Varian Cary 5 or a Cary 17 spectrophotometer with a spectral resolution of 0.04–0.2 nm and by using linearly polarized

light to register π and σ spectra. In order to get accurate values for the positions of the considered Stark levels, the experiments were performed at temperatures ranging between 4.2 and 40 K by using either a closed cycle or a He flow cryostat.

For the hole burning experiments, a Coherent CR-699-21 ring dye laser, pumped by a Spectra Physics 2080 argon-ion laser, was operated with Rhodamine 101. The dye laser had a spectral width of ∼1 MHz. The wavelength was calibrated by a Burleigh wavemeter (WA-4500). The laser beam was gated with an AA. Opto-electronics acousto-optic modulator (AOM) driven with a Tektronix AWG520 waveform generator. The laser output was split into two beams. One was used to irradiate the crystal and the other was used as a reference signal in order to eliminate the influence of fluctuations in the laser intensity. The light pulses were focused onto the crystal which was immersed in liquid helium and kept at a temperature of about 4 K. The focused beam had a diameter of ∼0.15 mm. A matched pair of electronically amplified photodiodes (Hamamatsu S1223) was then used for detecting the transmission hole spectrum and reference signal. A more detailed description can be found, for example, in [13].

3. Energy level calculations

Our calculations were performed by using a free ion Hamiltonian including the seven electrostatic and spin–orbit parameters which were obtained by Carnall *et al* [14] for trivalent rare-earth ions in aqueous solution, i.e. (all in cm^{-1}) $E^{(1)} = 6440.6$, $E^{(2)} = 30.22$, $E^{(3)} = 624.39$, $\xi = 2141.3$, $\alpha = 23.635$, $\beta = -807.2$ and $\gamma = 1278.4$, this Hamiltonian being written in the usual form [15]:

$$H_{fi} = \sum_K E^{(K)} e_K + \xi \sum_i \vec{s}_i \cdot \vec{l}_i + \alpha L(L+1) + \beta G(G_2) + \gamma G(R_7).$$

Since the local site symmetry of the Ho^{3+} ion in YVO_4 is D_{2d}, we chose a crystal-field Hamiltonian of the form

$$H_{cf} = B_2^0 C_2^0 + B_4^0 C_4^0 + B_4^4 [C_4^4 + C_4^{-4}] + B_6^0 C_6^0 + B_6^4 [C_6^4 + C_6^{-4}].$$

Three sets of B_k^q crystal-field parameters were then used. One set (labelled further set no. 1) was derived by using the data reported in [16]. These parameters were obtained by scaling the B_q^k parameters for Nd^{3+} in YVO_4 by the same variations of the B_q^k parameters that were used to scale the lanthanide series in the case of the isostructural compound YPO_4. This gives the B_k^q(Nd), B_k^q(Ho) and B_k^q(Er) parameters reported in table 1. A second set was derived by using the same ratio as above between the B_k^q(Ho) and B_k^q(Er) but starting with the B_k^q(Er) obtained for Er^{3+}:YVO_4 and reported in [17]. The third set was constructed in the same way but starting with the B_k^q(Nd) parameters obtained for Nd^{3+}:YVO_4 and reported in [18]. Finally, the fourth set of parameters (set no. 4) is the one reported in [19] to describe some magnetic properties of $HoVO_4$. All these parameters are gathered in table 1. The set labelled no. 5 will be discussed below.

4. Experimental results and discussions

Two types of spectra were registered in the case of Ho^{3+}:YVO_4:

(i) polarized absorption spectra recorded at various temperatures (10, 35, 71 and 298 K) in the wavelength domains of the $^5I_8 \rightarrow {}^5S_2$, $^5F_4$ and $^5I_8 \rightarrow {}^5F_5$ optical transitions around 645 nm (15 500 cm^{-1}) and 540 nm (18 520 cm^{-1}), respectively, and

(ii) low-temperature (10 K) emission spectra around 545 nm (18 450 cm^{-1}) corresponding to the reverse transition $^5S_2 \rightarrow {}^5I_8$.

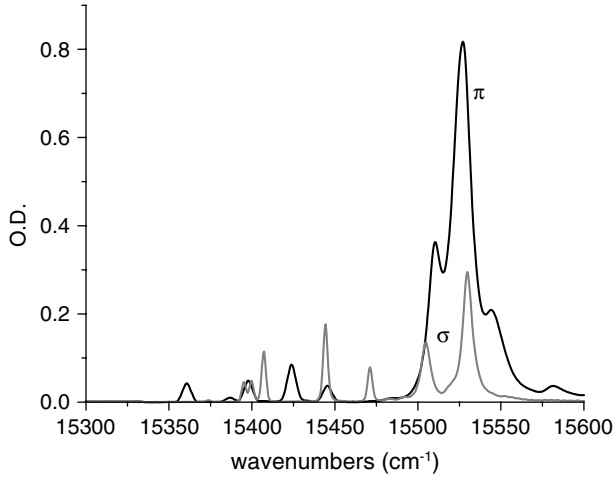

Figure 1. Low-temperature polarized absorption spectra of a 1% Ho^{3+}:YVO_4 crystal in the region of the $^5I_8 \rightarrow {}^5F_5$ inter-multiplet optical transition.

Table 1. Various sets of B_k^q parameters (in units of cm^{-1}).

	B_2^0	B_4^0	B_4^4	B_6^0	B_6^4
Nd [16]	−136	612	1044	−1186	−251
Er [16]	−92	190	671	−812	−169
Ho set no. 1	−97	245	718	−859	−179
Er [17]	−216	196	907.7	−682	37.1
Ho set no. 2	−227	252	971	−721	−39
Nd [18]	−200	628	1136	−1233	−149
Ho set no. 3	−142	251	772	−887	−106
Ho set no. 4 [19]	−164	302	∓890	−740	±114
Ho set no. 5	−230	280	750	−720	−150

These spectra were registered for 0.5% as well as for 1% Ho^{3+}-doped samples. Two of the absorption spectra are shown in the figures 1 and 2. It is worth noting here that it is the first time that these (rather complicated) spectra are shown in the literature. It is likely that the complexity of the spectra is the reason why such different assignments of the lines have been reported.

Our analysis of these spectra was based both on the examination of the temperature behaviour of each observed line but also by confronting their assignments with their expected positions and polarizations as they can be derived from the crystal-field calculations. Performing this procedure back and forth, we rapidly concluded that most of the energy level positions reported in [8] could not be confirmed since the Stark splittings of the considered multiplets were likely much lower than reported in that paper.

Although the different calculations produced somewhat different results, these calculations at least indicate that the maximum splittings of the levels $^5I_8$, $^5F_5$, $^5S_2$ and $^5F_4$ should not exceed about 310, 170, 26 and 100 cm^{-1} respectively. Except for $^5I_8$, these splittings, as mentioned above, are much more reduced than those reported in [8]. They agree better with the data reported in [7]. Considering these expected energy level positions and examining the temperature behaviour as well as the sample to sample variations of the lines, we ended

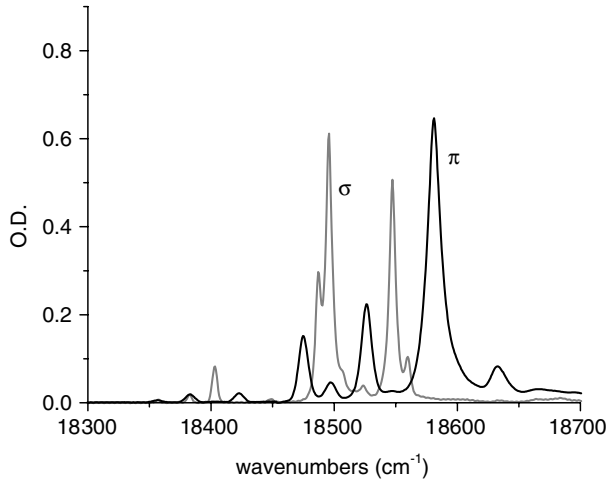

Figure 2. Low-temperature polarized absorption spectra of a 1% Ho^{3+}:YVO_4 crystal in the region of the $^5I_8 \rightarrow {}^5S_2$, $^5F_4$ inter-multiplet optical transition.

up with the experimental energy level positions reported as 'present experimental data' in table 2. The assignment of the observed lines was based on the selection rules for the optical transitions reported in table 3 (in which we also give the correspondence between the D_{2d} site symmetry irreducible representations Γ and the crystal quantum numbers μ). In table 2 we also give the positions of the energy levels resulting from calculations made by using a fifth set of crystal-field parameters (set no. 5 reported in table 1) adjusted to give a better agreement with the experimental data (those of [7] and ours).

Though our data agree better with those reported in [7] there are, however, substantial differences concerning the overall Stark splittings of the $^5S_2$ and $^5F_4$ multiplets and the symmetry (derived from the line polarizations) of the two lowest Stark components of the $^5F_4$ multiplet. These two points remain puzzling. First, concerning the $^5S_2$ multiplet, the calculations, whatever crystal-field parameter set is used, always indicate, as mentioned above, an overall crystal-field splitting not exceeding about 26 cm^{-1}, in agreement with the data of [7]. Our data, though not ambiguous, indicate instead 39 cm^{-1}. Second, concerning the $^5F_4$ multiplet, our experimental data differ from those given in [7] since they indicate slightly different level splittings and a lowest Stark level of Γ_1 symmetry. Such an inversion between the two lowest Stark components of the $^5F_4$ multiplet was indeed found to be possible through our calculations. It occurs, for example, by increasing the value of the B_6^4 parameter from -150 to 300 cm^{-1}. Consequently, some doubt exists concerning either the data reported in [7] or the real site symmetry of the Ho^{3+} ions in our samples (if the symmetry were different, the crystal-field Hamiltonian would not be the same and, in principle, could cause different level splittings).

The question thus remains partly open. However, it can be kept in mind that there is no ambiguity concerning the positions and the symmetry of the Stark components of the $^5I_8$ and $^5F_5$ multiplets, thus concerning the positions and the polarizations of the associated optical transitions the detail of which is reported in tables 4 and 5. From this point of view, our set of crystal-field parameters (set no. 5) seems more satisfactory than the one reported in [19] for $HoVO_4$.

Absorption spectra of the $^5I_8 \rightarrow {}^5F_5$ optical transition were also recorded at various temperatures in the case of the Ho^{3+}:$LuVO_4$ sample (figures 3 and 4). As expected from

Table 2. Results of crystal-field calculations and experimental data.

	$^5I_8$	$^5F_5$	$^5S_2$,$^5F_4$
Set no. 1	0, 12, 25, 57, 100, 103, 222, 225, 234, 236, 264, 278, 301	15 406.6+ 0, 3.5, 10, 44, 83, 114, 120, 133	18 388.7+ 0, 4.6, 5.5, 20.3, 18 489.3+ 0, 1.3, 43.5, 51.1, 62.5, 82.9, 89.7
Set no. 2	0, 17, 37, 52, 107, 143, 222, 236, 239, 242, 264, 270, 300	15 393.8+ 0, 4.4, 10, 52, 94, 161, 163, 170	18 386.7+ 0, 4.7, 9, 26.1, 18 498.3+ 0, 14.7, 25.8, 48.9, 58.5, 63.5, 96
Set no. 3	0, 17, 27, 59, 102, 118, 224, 235, 253, 253, 270, 283, 309	15 409.9+ 0, 2.3, 11, 44.5, 86, 124, 129, 141	18 394.3+ 0, 4.6, 6.4, 21.6 18 495.6+ 0, 6.2, 40.3, 55.2, 57, 81.3, 98.1
Set no. 4 (calculations made with parameters of [19])	0, 19.6, 43.4, 43.4, 113, 129.4, 222.8, 230.7, 231.6, 231.6, 261.6, 266.4, 297.4	15 296.2+ 0, 4.9, 9.7, 50.9, 95.1, 146.1, 150.2, 159.2	18 386.7+ 0, 4.6, 6.9, 24 18 495.6+ 0(Γ_5), 8.2(Γ_1), 33.2(Γ_2), 53.9, 55.8, 67.8, 89.6
[7] data	0(Γ_1), 20.7(Γ_5), 46.5(Γ_5), 46.5(Γ_4), ...	15 401.1+ 0(Γ_5), 10(Γ_3), 13.5(Γ_2), 37(Γ_5), 85(Γ_1), 118(Γ_4), 122(Γ_5), 132.5(Γ_2)	18 386.9+ 0(Γ_3), 7.2(Γ_1), 7.5(Γ_5), 26.5(Γ_4) 18 486.4+ 0(Γ_5), 12(Γ_1), 32.5(Γ_2), 49(Γ_1), 52(Γ_5), 71.5(Γ_3), 85(Γ_4)
Present experimental data	0(Γ_1), 20(Γ_5), 45(Γ_5),...	15 407+ 0(Γ_5), 11(Γ_3), 13(Γ_2), 36(Γ_5), 84(Γ_1), 119(Γ_4), 123(Γ_5), 131(Γ_2)	18 383+ 0(Γ_3), 20(Γ_1), 20(Γ_5), 39(Γ_4) 18 468+ 0(Γ_1), 27(Γ_5), 38(Γ_2), 49(Γ_1), 78(Γ_5), 101(Γ_3), 112(Γ_4)
Set no. 5	0, 20.5, 46.8, 48.5, 117.2, 122.8, 215.9, 216.9, 230.1, 232.2, 251.2, 255.8, 282.7	15 407.4+ 0, 10.3, 11.7, 38.5, 79.4, 124.8, 128.7, 137.5	18 384.3+ 0, 0.1, 3.3, 21 18 470.1+ 0, 11.8, 24.4, 48.1, 54.7, 68.1, 83.9

Table 3. Selection rules for optical transitions (π for $E \parallel c$, σ for $E \perp c$, R_z for $H \parallel c$, — for forbidden).

	$\Gamma_1, \mu = 0$	$\Gamma_2, \mu = 0$	$\Gamma_3, \mu = 2$	$\Gamma_4, \mu = 2$	$\Gamma_5, \mu = \pm 1$
$\Gamma_1, \mu = 0$	—	R_z	—	π	σ
$\Gamma_2, \mu = 0$	R_z	—	π	—	σ
$\Gamma_3, \mu = 2$	—	π	—	R_z	σ
$\Gamma_4, \mu = 2$	π	—	R_z	—	σ
$\Gamma_5, \mu = \pm 1$	σ	σ	σ	σ	π, R_z

the high J-value of these multiplets, a complex structure appears already at 40 K. As in the case of Ho^{3+}:YVO_4, assignment of the transitions to crystal-field levels and comparison with calculations is not straightforward. Since the spectra obtained with this system are similar to those recorded with Ho^{3+}:YVO_4, a similar crystal-field scheme was used (energy and irreducible representations) in order to account for our experiments (table 6). It appears however that this is not completely satisfactory, especially for the π polarized spectra: the line

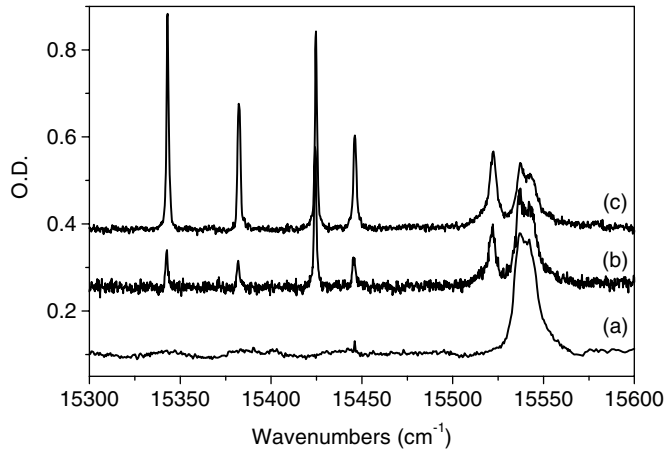

Figure 3. π polarized absorption spectra of a 1% Ho^{3+}:$LuVO_4$ crystal in the region of the $^5I_8 \rightarrow {}^5F_5$ inter-multiplet optical transition. (a) $T = 4.7$ K (spectral resolution 0.18 nm), (b) $T = 20$ K (resolution 0.04 nm), (c) $T = 40$ K (resolution 0.04 nm).

Table 4. Assignments of the observed lines for the $^5I_8 \rightarrow {}^5F_5$ optical transitions (exponents stand for observed line numbers by order of increasing energies; dash means forbidden transitions).

	Γ_5	Γ_3	Γ_2	Γ_5	Γ_1	Γ_4	Γ_5	Γ_3
Γ_1	$15\,407^7$	—	R_z	$15\,443^9$	—	$15\,526^{16}$	$15\,530^{17}$	—
Γ_5	$15\,387^3$	$15\,396^4$	$15\,400^5$	$15\,423^8$	$15\,471^{10}$	$15\,505^{13}$	$15\,510^{14}$	$15\,518^{15}$
Γ_5	$15\,361^1$	$15\,374^2$	$15\,375^2$	$15\,398^6$	$15\,444.5^9$	$15\,480.5^{11}$	$15\,484^{11}$	$15\,493^{12}$
Γ_4	?	R_z	—	$15\,400^5$	$15\,445^9$	—	$15\,484^{11}$	R_z

Table 5. Assignments of the observed lines for the $^5I_8 \rightarrow {}^5S_2$, $^5F_4$ optical transitions.

	Γ_3 ($^5S_2$)	Γ_1 ($^5S_2$)	Γ_5 ($^5S_2$)	Γ_4 ($^5S_2$)	Γ_1 ($^5F_4$)	Γ_5 ($^5F_4$)	Γ_2 ($^5F_4$)	Γ_1 ($^5F_4$)	Γ_5 ($^5F_4$)	Γ_3 ($^5F_4$)	Γ_4 ($^5F_4$)
$\Gamma_1(^5I_8)$	—	—	18 403	18 422	—	18 495	18 506	—	18 546	—	18 580
$\Gamma_5(^5I_8)$	18 358	18 383	18 383	18 402	18 448	18 475	18 486	18 497	18 526	18 549	18 560
$\Gamma_5(^5I_8)$	?	18 358	18 358	?	18 450	18 423	?	18 472	18 500	18 524	?

Table 6. Energies (cm^{-1}) and irreducible representations (assuming D_{2d} point symmetry) of $^5I_8$ and $^5F_5$ multiplets of Ho^{3+} in $LuVO_4$. Γ_i stands for Γ_1, Γ_2 or Γ_3.

$^5I_8$	$0(\Gamma_1)$	$22(\Gamma_5)$	$65(\Gamma_5)$					
$^5F_5$	$15\,408(\Gamma_5)$	$15\,423(\Gamma_i)$	$15\,427(\Gamma_i)$	$15\,447(\Gamma_5)$	$15\,497(\Gamma_i)$	$15\,513(\Gamma_i)$	$15\,541(\Gamma_4)$	$15\,545(\Gamma_5)$

around 15 540 cm^{-1} clearly has two components instead of one, the line at 15 547.5 cm^{-1} is unassigned and the $^5I_8(2) \rightarrow {}^5F_5(8)$ transition at 15 476 cm^{-1} is not observed experimentally. However, no better set of crystal-field levels could be found. Further investigations, including emission spectra at low and different temperatures, are needed to completely solve these problems. However, the energy differences between the first two crystal-field levels of the $^5I_8$ and $^5F_5$ multiplets seem reliable.

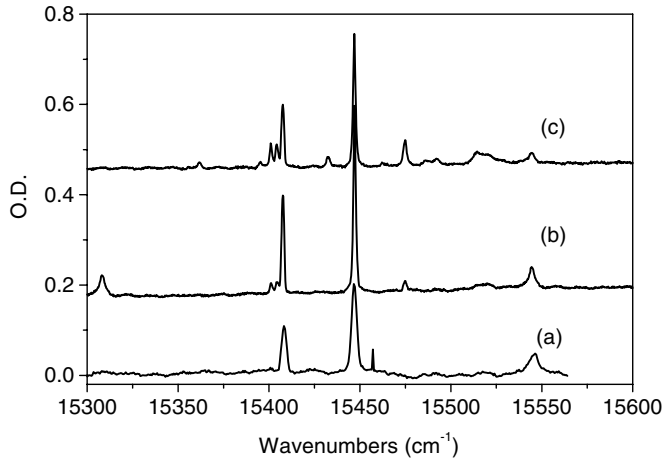

Figure 4. σ polarized absorption spectra of a 1% Ho^{3+}:$LuVO_4$ crystal in the region of the $^5I_8 \rightarrow {}^5F_5$ inter-multiplet optical transition. (a) $T = 4.7$ K (spectral resolution 0.18 nm), (b) $T = 20$ K (resolution 0.04 nm), (c) $T = 40$ K (resolution 0.04 nm).

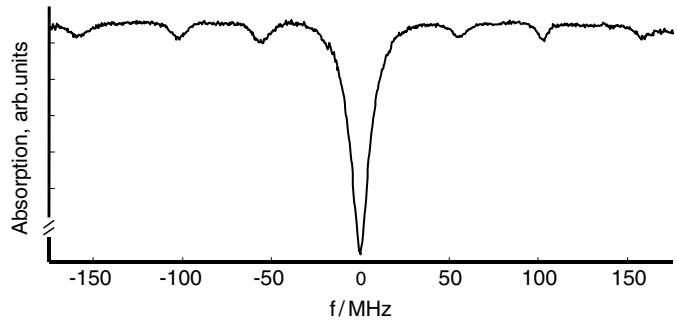

Figure 5. Partial hole burning spectrum in Ho^{3+}:YVO_4.

Spectral hole measurements were performed on the lowest Stark components of the zero-phonon $^5I_8(1)$–$^5F_5(1)$ transitions at 648.95 and 649.01 nm (15 409.5 and 15 408.1 cm^{-1}) for the Ho^{3+}:YVO_4 and Ho^{3+}:$LuVO_4$ single crystals, respectively. The spectral holes were probed by measuring the transmission of the laser with the intensity reduced by 2–3 orders of magnitude relative to the burning intensity. The burning pulse duration was varied from 0.5 to 10 ms. The readout pulse was scanned over 50–200 MHz in the spectral vicinity of the burning pulse and had a pulse duration ranging between 20 and 200 μs. The laser was continuously scanned over 1 GHz at a slow rate of about 200 MHz s^{-1} in order to avoid spectral overlap of the burning pulses while still ensuring that the reading pulse scanned the spectral vicinity of the burning pulse. The homogeneous linewidths of the $^5I_8(1)$–$^5F_5(1)$ optical transition were directly determined from the burned spectral hole. As an example, figure 5 illustrates a typical hole spectrum of Ho^{3+}:YVO_4. By adjusting the experimental conditions, for example, the duration of burning pulse and the separation between the burning and reading pulses, the minimum full width at half maximum (FWHM) of the holes was measured to be 20.4 and 15 MHz for Ho^{3+}:$LuVO_4$ and Ho^{3+}:YVO_4, respectively. According to the relation $\Gamma_{\text{hole}} = 2(\Gamma_h + \Gamma_{\text{laser}})$, the homogeneous linewidths can be determined to be 8.5 and 6.5 MHz

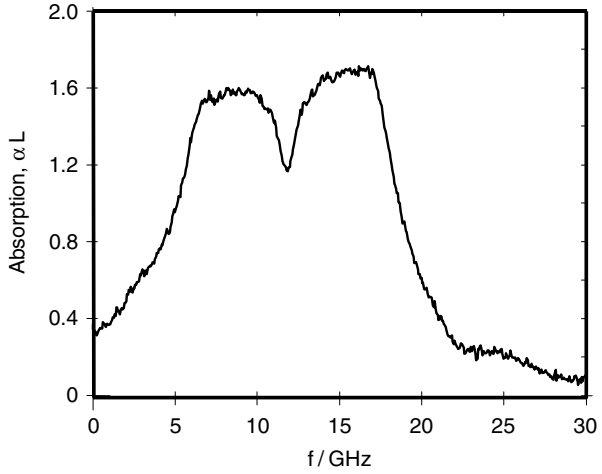

Figure 6. Inhomogeneous absorption profile in Ho^{3+}:YVO_4.

Table 7. The spectral parameters obtained for the two crystals.

	Ho^{3+}:YVO_4	Ho^{3+}:$LuVO_4$
$\lambda[^5I_8(1)–^5F_5(1)]$	648.95 nm	649.01 nm
Γ_{hom}	6.5 ± 0.5 MHz	8.5 MHz
Γ_{inhom}	14.5 ± 0.5 GHz	>20 GHz
T_2	49 ± 4.5 ns	37 ± 3.4 ns
T (Hole lifetime)	1.0 ± 0.2 ms	311 ± 27 μs

for Ho^{3+}:$LuVO_4$ and Ho^{3+}:YVO_4, respectively. The dephasing time T_2, which is related to Γ_h by $\Gamma_h = 1/(\pi T_2)$, can thus be determined to be 37 and 49 ns for the $^5I_8(1) \rightarrow {}^5F_5(1)$ transition in the Ho^{3+}:$LuVO_4$ and Ho^{3+}:YVO_4 crystals, respectively. The homogeneous linewidths and dephasing times of the two crystals are listed in table 7. The large homogeneous linewidths Γ_h may arise from ion–host interaction, that is, spin fluctuations (random flipping of the nuclear magnetic spins of the host ions). This interpretation is supported by the fact that the constituents of the host material, YVO_4 and $LuVO_4$, have relatively high nuclear magnetic moments. The main contribution comes from ^{51}V, with an isotope abundance of 99.75% and a nuclear magnetic moment of 5.16 μ_N. It can also be noted that the element Lu (^{175}Lu, 97.41% abundance) has a higher nuclear magnetic moment, i.e., 2.23 μ_N, than that (-0.14 μ_N) of the element Y (^{89}Y, 100% abundance), which could be a reason for a larger homogeneous linewidth in Ho^{3+}:$LuVO_4$ than in Ho^{3+}:YVO_4, as is experimentally observed. However, for a more detailed explanation, it could be helpful to carry out an experimental measurement with an external magnetic field which could decrease the host–ion spin flip rate. Another reason for the short dephasing times could be a strong enhanced nuclear Zeeman effect due to small crystal-field level splittings [20]. However, the values that we found for the first three levels of the $^5F_5$ multiplet in both compounds are in the 13–20 cm^{-1} range, which is relatively large.

In these experiments, the inhomogeneous linewidths were also measured by scanning the single frequency dye laser and recording the absorption spectra. The results are 14.5 GHz and >20 GHz for Ho^{3+}:YVO_4 and Ho^{3+}:$LuVO_4$, respectively (see in table 7). The estimated value (>20 GHz) is due to the limited scanning range of our dye laser. Figure 6 shows the absorption line shape found in the case of Ho^{3+}:YVO_4, in which a puzzling doublet structure

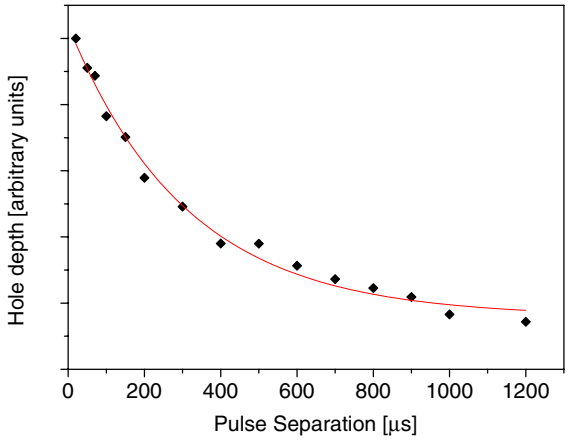

Figure 7. Hole depth as a function of time duration between burning and reading pulses in Ho^{3+}:$LuVO_4$.

(This figure is in colour only in the electronic version)

was observed. The reason for this unusual line profile is not known, but it could be due, in principle, to the superposition of inhomogeneously broadened transitions from different ground-state hyperfine levels, separated by several GHz. The slight asymmetry of the line shape in figure 6 could be explained by the thermal population difference between these levels at 4 K.

After the hole was burned in the absorption line, the spectral hole lifetimes were also measured by scanning the laser frequency with intensity attenuated by a factor of 10^3–10^4 in order to avoid the influence of the probe laser on the hole decay. As an example, the spectral hole depth as a function of time separation between the burning and probing laser pulses in Ho^{3+}:$LuVO_4$ is illustrated in figure 7. A single exponential fit gives a time constant of 311 μs. The results are listed in table 7.

As generally performed [13, 21], the hyperfine structures were directly determined by recording the transmission hole spectra. Due to the presence of the inhomogeneous broadening, all the allowed transitions between the hyperfine levels of the ground and excited states are resonant with the frequency of the burning laser for some subset of ions and a pattern of side holes and anti-holes could thus be recorded. The side holes are due to transitions from the hyperfine levels with depleted population in the ground state to all of the excited state hyperfine levels. On the other hand, the anti-holes are due to population redistribution between the ground-state hyperfine levels, giving rise to enhanced absorption features. The Ho nucleus has a spin $I = 7/2$ and the nuclear quadrupole interaction and the second-order hyperfine coupling result in four hyperfine levels with $I_z = \pm 1/2, \pm 3/2, \pm 5/2, \pm 7/2$. In this case, a pattern of 6 sideholes and 52 antiholes on each side of the burning laser frequency (primary hole) are expected. As shown in figure 5, 6 sideholes were effectively observed in Ho^{3+}:YVO_4. The frequencies of the excited-state splittings are determined to be $\delta = \pm 55$, ± 103 and ± 159 MHz. However, no antiholes were observed. For Ho^{3+}:$LuVO_4$, no information on sideholes or antiholes were obtained, which might be because the signals were too weak. The frequency intervals between the primary hole and the sideholes give the hyperfine level splittings of the excited state, whereas the frequency intervals between the primary hole and the antiholes yield the hyperfine level splittings of the ground state. Therefore, the values of the side-hole splittings in figure 5 reveal that the hyperfine level separations in the excited

state are of the order of 50–100 MHz in Ho^{3+}:YVO_4. The results could possibly support the previous assumption that the different ground-state hyperfine levels are separated by several GHz, resulting in the puzzling doublet structure of the absorption line shape observed in Ho^{3+}:YVO_4.

5. Conclusion

A new analysis of Ho^{3+} crystal-field levels in YVO_4 has been performed for the $^5I_8$, $^5F_5$, $^5F_4$ and $^5S_2$ multiplets using absorption and emission spectra recorded at several temperatures. Since previous works showed significant discrepancies, crystal-field level calculations were also used to assign experimentally derived energy levels. Finally, a reasonable agreement has been obtained between calculated and experimental crystal-field level positions and irreducible representation labelling. However, analysis of the $^5F_4$ and $^5S_2$ multiplets suggests that the local site symmetry of Ho^{3+} may slightly deviate from D_{2d}. Similar spectra and level assignments were found for the isostructural compound Ho^{3+}:$LuVO_4$. In this case, too, it seems that the exact local site symmetry of Ho^{3+} may not be exactly D_{2d} since some lines could not be attributed.

Motivated by the search for good rare-earth candidates as active ions for quantum computing in inorganic crystals, the homogeneous line widths and associated dephasing times for the zero-phonon $^5I_8(1)$–$^5F_5(1)$ transitions were also measured for both crystals. Compared with the 100 μs–1 ms dephasing times found in other Pr^{3+} and Eu^{3+}-doped crystals [22, 23], the tens of ns dephasing times obtained in the case of Ho^{3+}:YVO_4 and Ho^{3+}:$LuVO_4$ probably makes them less suitable for quantum computing applications. These low values should not be due to a strong enhanced Zeeman effect since we have determined that the energy differences between the first levels of the $^5I_8$ and $^5F_5$ multiplets exceed 10 cm^{-1} in both compounds. Fast dephasing is therefore attributed to fluctuations of the high nuclear magnetic moment of the vanadium ions.

Acknowledgments

Thanks are expressed to Professor J Margerie and Dr J L Doualan from CIRIL laboratory for their assistance in some of the calculations and experiments. This work was partly supported by the ESQUIRE project within the IST-FET program of the EU, the Swedish Research Council and the Knut and Alice Wallenberg Foundation.

References

[1] Schellhorn M, Hirth A and Kieleck C 2003 *Opt. Lett.* **28** 1933 and references therein
[2] Pilawa B 1991 *J. Phys.: Condens. Matter* **3** 655
[3] McLeod D P and Reid M F 1997 *J. Alloys Compounds* **250** 302
[4] Dieke G H and Pandey B 1964 *J. Chem. Phys.* **41** 1952
[5] Wortman D E and Sanders D 1970 *J. Chem. Phys.* **53** 1247
[6] Kaminskii A A 1981 *Laser Crystals, Their Physics and Properties* (Berlin: Springer) p 1990
[7] Enderle M, Pilawa B, Schlaphof W and Kahle H G 1990 *J. Phys.: Condens. Matter* **21** 4685
[8] Golab S, Solarz P, Dominiak-Dzik G, Lukasiewicz T, Swirkowicz M and Ryba-Romanowski W 2002 *Appl. Phys.* B **74** 237
[9] Ohlsson N, Krishna Mohan R and Kröll S 2002 *Opt. Commun.* **201** 71–7
[10] Könz F, Sun Y, Thiel C W, Cone R L, Equall R W, Hutcheson R L and Macfarlane R M 2003 *Phys. Rev.* B **68** 085109
[11] http://www.webelements.com

[12] Garton G, Smith S H and Wanklyn B M 1972 *J. Cryst. Growth* **13/14** 588
[13] Xu H L, Nilsson M, Ohser S, Rauhut N, Kröll S, Aguiló M and Díaz F 2004 *Phys. Rev.* B **70** 214115
[14] Carnall W T, Fields P R and Rajnak K 1968 *J. Chem. Phys.* **49** 4412
[15] Carnall W T, Goodman G L, Rajnak K and Rana R S 1989 *J. Chem. Phys.* **90** 3443
[16] Karayianis N, Wortman D E and Morrison C A 1976 Rare-earth ion–host lattice interactions, 7. Lanthanides in YVO_4 *Harry Diamond Lab. Report* HDL-TR-1775
[17] Capobianco J A, Kabro P, Ermeneux F S, Moncorgé R, Bettinelli M and Cavalli E 1997 *Chem. Phys.* **214** 329
[18] Guillot-Noël O, Kahn-Harari A, Viana B, Vivien D, Antic-Fidancev E and Porcher P 1998 *J. Phys.: Condens. Matter* **10** 6491–803
[19] Skanthakumar S, Loong C K, Soderholm L, Abraham M M and Boatner L A 1995 *Phys. Rev.* B **51** 12451
[20] Macfarlane R and Shelby R 1987 *Spectroscopy of Solids Containing Rare Earth Ions* (Amsterdam: North-Holland) chapter 3, pp 51–184
[21] Babbitt W R, Lezama A and Mossberg T W 1989 *Phys. Rev.* B **39** 1987
[22] Equall R W *et al* 1994 *Phys. Rev. Lett.* **72** 2179
[23] Equall R W *et al* 1995 *Phys. Rev.* B **52** 3963